REVIEW

Review on second-harmonic generation of ultrasonic guided waves in solid media (I): Theoretical analyses*

Wei-Bin Li(李卫彬)[1], Ming-Xi Deng(邓明晰)[2,†], and Yan-Xun Xiang(项延训)[3,‡]

[1] School of Aerospace Engineering, Xiamen University, Xiamen 361005, China
[2] Department of Physics, Logistics Engineering University, Chongqing 401331, China
[3] School of Mechanical and Power Engineering, East China University of Science and Technology, Shanghai 200237, China

(Received 3 July 2017; revised manuscript received 31 July 2017; published online 30 September 2017)

Considering the high sensitivity of the nonlinear ultrasonic measurement technique and great advantages of the guided wave testing method, the use of nonlinear ultrasonic guided waves provides a promising means for evaluating and characterizing the hidden and/or inaccessible damage/degradation in solid media. Increasing attention on the development of the testing method based on nonlinear ultrasonic guided waves is largely attributed to the theoretical advances of nonlinear guided waves propagation in solid media. One of the typical acoustic nonlinear responses is the generation of second harmonics that can be used to effectively evaluate damage/degradation in materials/structures. In this paper, the theoretical progress of second-harmonic generation (SHG) of ultrasonic guided wave propagation in solid media is reviewed. The advances and developments of theoretical investigations on the effect of SHG of ultrasonic guided wave propagation in different structures are addressed. Some obscure understandings and the ideas in dispute are also discussed.

Keywords: second-harmonic generation (SHG), ultrasonic guided waves, cumulative growth effect, phase and group velocity matching

PACS: 43.20.Mv, 43.25.+y, 43.35.–c **DOI:** 10.1088/1674-1056/26/11/114302

1. Introduction

It is known that ultrasonic guided waves propagating in a body (waveguide) usually with at least two boundaries consist of multiple bulk waves, such as longitudinal and transverse/shear waves. Essentially, these bulk waves are obliquely reflected/refracted by each boundary, causing them to propagate back and forth in the waveguide.[1–6] Inevitably, the interference between them will take place. A steady interference pattern in the waveguide will appear once the interference is constructive in nature. The result of this effect is that propagating bulk waves are guided in a certain direction.

It is important to note that acoustic nonlinearity can be taken as any deviation from the linear law of the transformation of the input wave signal due to its propagation through a carrying system.[7] Thus, the acoustic nonlinear response of ultrasonic wave propagation in a solid may appear in the signal received at all stages starting from the position of excitation source, as well as the wave propagation in the elastic materials. The basic idea of nonlinear ultrasonic wave propagation in a medium is the generation of waves with multiple frequencies. The importance of studying nonlinear ultrasonic wave propagation is motivated by the fact that such waves generated can be excellent tools for analyzing different properties of materials in the early stage.[8–12] The use of nonlinear ultrasonic waves has been proposed as being one of the most promising methods for evaluating material damage/degradation in the early stage.[13–16] The principal investigation on nonlinear ultrasonic guided waves generally focuses on the analyses of generated waves whose frequency differs from that of the primary guided wave signal. Due to the convective nonlinearity independent of the material properties and the elastic nonlinearity in a solid, the distortion of ultrasonic guided wave propagation can cause the higher harmonic generation. One of the typical nonlinear phenomena is the generation of second harmonics.[17]

Compared to bulk waves, the effect of second-harmonic generation (SHG) of ultrasonic guided wave propagation is much more complex because of its dispersion and multimode features.[18,19] In general, the effect of SHG is tiny and easily overlooked due to the dispersive nature of guided waves. Meanwhile, the multimode feature makes it difficult to generate the single guided wave mode desired. Theoretical analyses of generation of second harmonics of ultrasonic guided waves can provide a guideline for practical applications of nonlinear ultrasonic guided waves.

A straightforward analysis of SHG of ultrasonic guided waves propagation can not only provide us with an insight into its physical process, but it also can enhance the understanding of technique based on nonlinear ultrasonic guided waves

*Project supported by National Natural Science Foundation of China (Grant Nos. 11474361, 51405405, and 11622430).
†Corresponding author. E-mail: dengmx65@yahoo.com
‡Corresponding author. E-mail: yxxiang@ecust.edu.cn
© 2017 Chinese Physical Society and IOP Publishing Ltd

for practical applications. In this paper, the features of multimode and dispersion of ultrasonic guided waves are firstly discussed to show the importance of suitable mode selection and frequency tuning for ultrasonic guided waves testing. Two general methods are provided in Section 3, for the analyses of nonlinear wave equations by the technique of nonlinear reflection of acoustic waves and modal analysis approach. The conditions for the generation of second harmonics with a cumulative effect are discussed in this section. The research advances of various types of nonlinear guided waves in different structures are reviewed in Section 4. In Section 5, the physical insight of the nonlinear feature of guided wave modes is provided to compare the efficiency of SHG of ultrasonic Lamb wave modes. The review in this paper focuses on the theoretical analyses of SHG of various types of ultrasonic guided wave modes in solid media. Discussions about some disputed issues are also provided.

2. Dispersion and multimode features of ultrasonic guided waves

Dispersion equations can be obtained by solving the equations of wave motion and enforcing the satisfactions of boundary conditions for wave propagation in the waveguide. Generally, solutions for the dispersion equations can only be found numerically.[20,21] Thus, the propagating guided wave modes can be depicted in phase velocity dispersion curves, as shown in Fig. 1(a). This derivative is again taken numerically and is referred to as group velocity

$$c_{\mathrm{g}} = 2\pi \frac{\partial f}{\partial k}. \tag{1}$$

The group velocity describes the velocity of the energy propagating with the wave and does therefore have a physical meaning. In contrast to that, the phase velocity $c_{\mathrm{p}} = 2\pi f/k$ refers to the velocity of points with the constant phase. Phase velocity dispersion curves help to choose the modes desired, and group velocity curves can be used to check the guided wave modes experimentally.

In general, an ultrasonic guided wave propagates as a wave packet containing a number of neighboring frequency components around the center frequency. The speed of the wave packet is called group velocity, while the phase velocity is the speed of phase shift of a pure single frequency wave mode. As shown in Fig. 1, the phase velocity of guided wave propagation is dependent on the driving frequency. For a given propagating guided wave mode, the phase velocity is not equal to the group velocity due to its dispersion nature.[22,23] It is also indicated that there are at least two guided wave modes at a certain driving frequency. That is the so-called multimode feature of guided waves propagation.

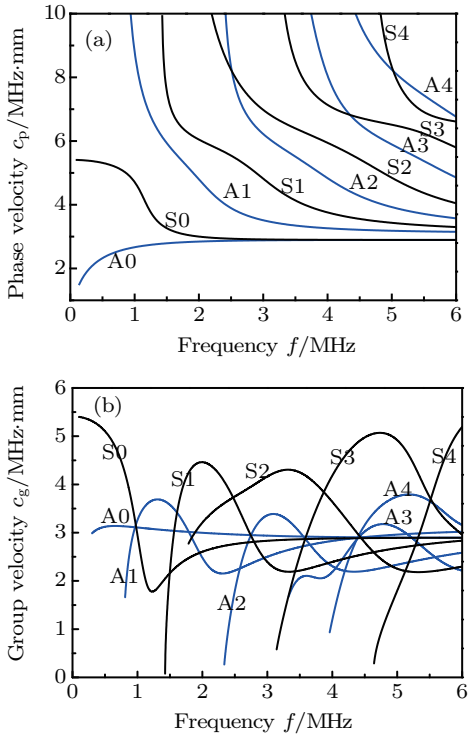


Fig. 1. (color online) Phase (a) and group (b) velocity dispersion curves of guided waves in an aluminum plate with 2 mm thickness.

3. Theoretical fundamentals

The nonlinear wave equation in Lagrangian coordinates is expressed as[24–28]

$$(\lambda + 2\mu)\nabla(\nabla \cdot \boldsymbol{u}) - \mu\nabla \times (\nabla \times \boldsymbol{u}) + \boldsymbol{f}(\boldsymbol{u}) = \rho_0 \frac{\partial^2 \boldsymbol{u}}{\partial t^2}, \tag{2}$$

where $\boldsymbol{u}$ is the particle displacement, λ and μ are the Lame constants, ρ_0 is the initial mass density of the material, and $\boldsymbol{f}(\boldsymbol{u})$ is the nonzero nonlinear term.

The perturbation method can effectively be used to solve the nonlinear wave equation, and thus the solution can be taken as the sum of the primary wave $\boldsymbol{u}_1$ and the second-order wave $\boldsymbol{u}_2$, i.e., $\boldsymbol{u} = \boldsymbol{u}_1 + \boldsymbol{u}_2$. For the case of SHG where the primary wave (fundamental frequency component) propagates in a waveguide, the primary wave and the second-order wave (double frequency component, i.e., second harmonic) are taken as a pair of waves which will separately satisfy the boundary conditions, with the assumption that $\boldsymbol{u}_2$ is much smaller than $\boldsymbol{u}_1$. Then, the nonlinear wave Eq. (2) can be decomposed into two linear equations, given by[29,30]

$$(\lambda + 2\mu)\nabla(\nabla \cdot \boldsymbol{u}_1) - \mu\nabla \times (\nabla \times \boldsymbol{u}_1) = \rho_0 \frac{\partial^2 \boldsymbol{u}_1}{\partial t^2}, \tag{3}$$

and

$$(\lambda + 2\mu)\nabla(\nabla \cdot \boldsymbol{u}_2) - \mu\nabla \times (\nabla \times \boldsymbol{u}_2) + \boldsymbol{f}(\boldsymbol{u}_1) = \rho_0 \frac{\partial^2 \boldsymbol{u}_2}{\partial t^2}, \tag{4}$$

where $\boldsymbol{f}(\boldsymbol{u}_1)$ as the driving force of $\boldsymbol{u}_2$ is computed from nonlinear term $\boldsymbol{f}(\boldsymbol{u})$ in Eq. (2), using $\boldsymbol{u}_1$ shown in Eq. (3) instead of $\boldsymbol{u}$.

To find the solution of second harmonics of primary guided wave propagation, two methods of theoretical analyses were successively used. First, Deng used the technique of nonlinear reflection of acoustic waves at an interface to derive the solutions of second harmonics of Lamb waves, and the investigations revealed the corresponding physical process of SHG.[27,28] Further, Deng derived the cumulative second-harmonic solution that could be used to effectively describe the distortion of the second-harmonic field patterns.[29] Subsequently, Deng and de Lima *et al*. separately used a combination of second-order perturbation approximation and modal expansion approach to develop a more general solution of second harmonics.[31,32]

The acoustic fields of second harmonics of Lamb wave propagation are considered as the superposition of a series of double frequency Lamb wave (DFLW) modes. The contribution of each DFLW component to the second-harmonic fields is mainly dependent on the difference between the phase velocities of the primary Lamb wave mode and that of the said DFLW, as well as the degree of energy coupling between them. The field of the DFLW component has a cumulative growth effect when its phase velocity exactly or approximately equals that of the primary Lamb wave mode and the energy coupling between them is not zero. The solutions obtained provide a physical insight of SHG of the Lamb wave with a cumulative growth effect. These investigations lay the basis for the theoretical development of SHG of ultrasonic guided waves.[27–32] The two methods of theoretical analysis of SHG will be briefly reviewed.

3.1. Analysis based on nonlinear reflection of acoustic waves

To study the effect of SHG of guided waves propagation, Deng first investigated the feature of the second-harmonic field of the Lamb wave propagation in an isotropic plate,[29] using the technique of nonlinear reflection of acoustic waves at an interface.[33,34] Primary Lamb wave propagation can be taken as the superposition of the four bulk wave modes (two longitudinal and two transverse waves) propagating in the plate, as described in Fig. 2.

The primary wave field of Lamb wave propagation can be expressed as

$$\boldsymbol{u}_1 = \boldsymbol{u}_{\mathrm{L1}} + \boldsymbol{u}_{\mathrm{T1}} + \boldsymbol{u}_{\mathrm{L2}} + \boldsymbol{u}_{\mathrm{T2}}, \tag{5}$$

where $\boldsymbol{u}_1$ satisfies Eq. (3). The stress-free boundary conditions determine the Lamb wave dispersion relations and the amplitudes of the four partial waves (two longitudinal waves $\boldsymbol{u}_{\mathrm{L1}}$ and $\boldsymbol{u}_{\mathrm{L2}}$, and two transverse waves $\boldsymbol{u}_{\mathrm{T1}}$ and $\boldsymbol{u}_{\mathrm{T2}}$), which require that the normal and tangential stress should be zero at the two surfaces of the plate.

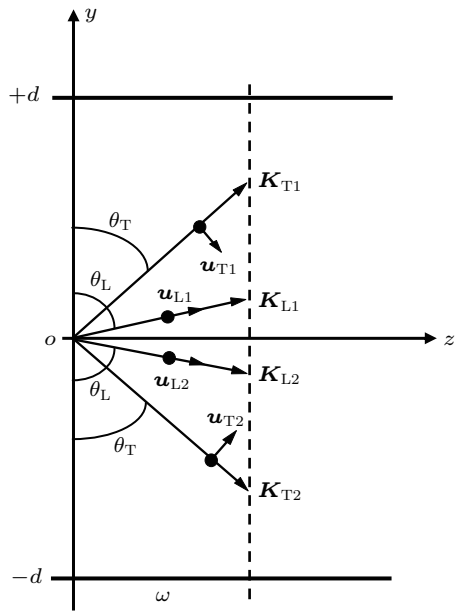


Fig. 2. Acoustic field of primary Lamb wave propagation in a plate.[29]

The acoustic field of second harmonic of primary Lamb wave propagation can be obtained by analyzing the self- and cross-interactions of the two longitudinal waves and two transverse waves. Through these complicated self- and cross-interactions, ten driven longitudinal second harmonics and four transverse second harmonics will be generated.[29,33–35] Generally, only the self-interaction of the primary longitudinal wave (i.e., $\boldsymbol{u}_{\mathrm{L1}}$ or $\boldsymbol{u}_{\mathrm{L2}}$) can generate the resonant (or cumulative) longitudinal second harmonic due to the phase velocity matching between the primary wave and the second harmonic generated. For each of the other driven second harmonics generated, due to the phase velocity mismatching, the efficiency of its generation is very inefficient. That is to say, the corresponding second-harmonic solution does not have a cumulative term.

The second-harmonic boundary condition at the two surfaces of the solid plate requires that the components of second-harmonic stress equal zero. Generally, this boundary condition cannot be satisfied if only the driven second harmonics are considered. In fact, these driven second harmonics (generated by $\boldsymbol{f}(\boldsymbol{u}_1)$ in Eq. (4)) are the particular solution to Eq. (4). The full solution to Eq. (4) should include both the particular and general solutions. When $\boldsymbol{f}(\boldsymbol{u}_1)$ in Eq. (4) is set to be zero, the general solution satisfying Eq. (4) can readily be obtained.[29] The general solution to Eq. (4) is also referred to as the freely-propagating second harmonic since there is no driving force. The boundary condition of second harmonics may be satisfied by taking into account both the particular and general solutions.

Based on the technique of nonlinear reflection of acoustic waves at an interface, the general solution to Eq. (4) can formally be determined, which includes the plane wave term,

as well as the cumulative wave term.[29,35] Through solving the equation of the boundary condition where the second-harmonic stresses arising from the driven and the freely-propagating second harmonics are zero at the two surfaces, the solution to the freely-propagating second harmonics can be derived. Especially for the case of phase velocity matching between the primary and double frequency Lamb wave modes, the solution to the cumulative second harmonic (consisting of the driven and the freely-propagating cumulative second harmonics) of primary Lamb wave propagation can be determined, which satisfies the wave equation, boundary, and initial conditions of excitation.

The above analysis based on the technique of nonlinear reflection of acoustic waves at an interface is straightforward and convenient for understanding the physical process of the nonlinear guided waves propagation in solid media. In addition, the solution derived is relatively easy for numerical computations and can also be readily used to demonstrate the influence of the location of the excitation source on the second-harmonic field. However, the solution derived by this method is relatively complex and cumbersome, and it is not applicable to the case where the phase velocity matching is approximately satisfied, as well as the case where ultrasonic guided waves propagate in anisotropic media or waveguides with arbitrary geometries. To avoid these deficiencies, Deng and de Lima *et al.* separately adopted the modal expansion analysis approach to investigate the secondary wave field of guided wave propagation within a perturbation approximation.[31,32]

3.2. Analyses based on normal modal expansion approach

According to the modal analysis approach, the solution of acoustic field generated by the surface traction $\boldsymbol{s}$ and the volume force $\boldsymbol{f}$ in a plate can be written as a linear combination of normal guided wave modes[3]

$$\boldsymbol{u} = \frac{1}{2}\sum_m A_m(z)\boldsymbol{u}_m(y)\exp(-\mathrm{j}\omega t), \tag{6}$$

where $\boldsymbol{u}_m(y)$ is the displacement field function of the mth guided wave mode, and $A_m(z)$ is the corresponding expansion coefficient, and 1/2 is multiplied to ensure real quantities. $A_m(z)$ is the solution of the ordinary differential equation

$$4P_{mn}\left(\frac{\mathrm{d}}{\mathrm{d}z}+\mathrm{j}k_n^*\right)A_m(z) = (f_n^{\mathrm{surf}}+f_n^{\mathrm{vol}})\exp-\mathrm{j}\omega(t), \tag{7}$$

where

$$P_{mn} = -\frac{1}{4}\int_\Omega (\boldsymbol{v}_n^*\cdot\boldsymbol{s}_m+\boldsymbol{v}_m\cdot\boldsymbol{s}_n^*)\cdot\boldsymbol{n}_z\mathrm{d}\Omega, \tag{8}$$

$$f_n^{\mathrm{surf}}(z) = \int_\Gamma \boldsymbol{v}_n^*\cdot\boldsymbol{s}\cdot\boldsymbol{n}_z\mathrm{d}\Gamma, \tag{9}$$

$$f_n^{\mathrm{vol}}(z) = \int_\Omega \boldsymbol{v}_n^*\cdot\boldsymbol{f}\,\mathrm{d}\Omega, \tag{10}$$

where $\boldsymbol{v} = \partial\boldsymbol{u}/\partial t$, Ω is the waveguide cross-sectional area, and Γ is the curve enclosing Ω. The terms $f_n^{\mathrm{surf}}(z)$ and $f_n^{\mathrm{vol}}(z)$ are defined as the complex external power due to the surface traction $\boldsymbol{s}$ and the volume force $\boldsymbol{f}$ of ultrasonic guided waves, respectively. k_n is the wavenumber of the wave mode that is not orthogonal to the mode with the wavenumber k_m.

Generally, the normal modal analysis approach is based on the reciprocity relation, while the reciprocity theory cannot be used to analyze the nonlinear problem. However, under a second-order perturbation, the acoustic nonlinear response can be considered as a perturbation to primary wave motion. Thus, the SHG of ultrasonic guided wave propagation can be taken as a linear response with the given excited sources due to propagation of primary guided waves.

The acoustic field of the second harmonic generated can be constructed via this modal expansion approach. By using the normal mode expansion approach, the second-harmonic field of Lamb wave propagation can be considered as a linear summation of a series of DFLW modes. However, it is inconvenient for numerical computations by employing the normal modal analysis approach to analyze the second harmonic field of guided waves propagation. Considering the complexity of nonlinear guided waves, combining the nonlinear reflection of acoustic waves at interfaces and normal modal expansion can be used to understand the physical insight and propagation procedure of SHG of guided waves. A straightforward approach for analysis of DFLWs by using the partial wave technique and modal analyses approach was proposed by Deng.[36] As described in Fig. 2, the Lagrangian coordinates are established for a solid plate with a thickness of $2d$. The lth Lamb wave mode consists of the four partial bulk waves, denoted by the four displacement vectors $\boldsymbol{u}_{(l)\mathrm{Li}}$ and $\boldsymbol{u}_{(l)\mathrm{Ti}}$ ($i = 1, 2$). The field of the lth Lamb wave is given by $\boldsymbol{u}_{(l)}^{(f)} = \sum_i[\boldsymbol{u}_{(l)\mathrm{Li}}+\boldsymbol{u}_{(l)\mathrm{Ti}}]$. There is a bulk driving force with the double frequency $2f$, denoted by $\boldsymbol{F}_{\mathrm{b}}^{(2f)} = \boldsymbol{F}(\boldsymbol{u}_{(l)}^{(f)})$, in the solid plate due to the elastic nonlinearity of the plate material. Besides, there are second-order stress tensors with the double frequency $2f$ at the two surfaces of the solid plate, denoted by $\boldsymbol{P}_{\mathrm{s}}^{(2f)}$ and obtained through the first Piola–Kirchhoff stress tensor formula.[36] The total second-harmonic field of the lth Lamb wave can be expressed by the summation of a series of DFLWs, i.e., $\boldsymbol{u}^{(2f)} = \sum_n \boldsymbol{u}_{(n)}^{(2f)}(y,z) = \sum_n A_n(z)\boldsymbol{u}_n^{(2f)}(y)$, where $\boldsymbol{u}_{(n)}^{(2f)}(y)$ is the field function of the nth DFLW, and $A_n(z)$ is the corresponding expansion coefficient. The equation governing $A_n(z)$ is given by

$$\begin{aligned} 4P_{nn}\left(\frac{\partial}{\partial z}-\mathrm{j}k_{(n)}^{(2f)}\right)A_n(z) &= F_{(n)},\\ F_{(n)} &= \mathrm{j}2\omega\tilde{\boldsymbol{u}}_{(n)}^{(2f)}(y)\cdot\boldsymbol{P}_{\mathrm{s}}^{(2f)}\cdot\hat{\boldsymbol{y}}\Big|_{y=-d}^{y=d}\\ &\quad+\int_{-d}^{d}\mathrm{j}2\omega\tilde{\boldsymbol{u}}_{(n)}^{(2f)}(y)\cdot\boldsymbol{F}_{\mathrm{b}}^{(2f)}\mathrm{d}y, \end{aligned} \tag{11}$$

where P_{nn} is the average power flow per unit width along the x axis for the nth DFLW; $k_{(l)}^{(f)}$ and $k_{(n)}^{(2f)}$ are respectively the oz-axis components of the wave vectors of the bulk waves constituting the lth Lamb wave (namely $\boldsymbol{u}_{(l)}^{(f)}$) and the nth DFLW; $\hat{\boldsymbol{y}}$ is the oy-axis unit vector; $c_{(l)}^{(f)} = \omega/k_{(l)}^{(f)}$ and $c_{(n)}^{(2f)} = 2\omega/k_{(n)}^{(2f)}$ are the phase velocities of the lth Lamb wave and the nth DLFW, respectively. The sign $\sim$ on the top of $\boldsymbol{u}_{(n)}^{(2f)}(y)$ denotes the complex conjugate operation. Combining the initial condition of SHG with Eq. (13) yields the formal solution of $A_n(z)$

$$A_n(z) = \frac{F_{(n)}z}{4P_{nn}}\left\{\frac{\sin[(k_{(l)}^{(f)} - k_{(n)}^{(2f)}/2)z]}{[k_{(l)}^{(f)} - k_{(n)}^{(2f)}/2]z} \times \exp\left[\mathrm{j}(k_{(l)}^{(f)} - k_{(n)}^{(2f)}/2)z\right]\right\}\exp[\mathrm{j}k_{(n)}^{(2f)}z]. \quad (12)$$

It is found that $A_n(z)$ may be linearly proportional to propagation distance z when both the conditions $F_{(n)} \neq 0$ and $k_{(l)}^{(f)} = k_{(n)}^{(2f)}/2$ (namely phase velocity matching $c_{(l)}^{(f)} = c_{(n)}^{(2f)}$) are satisfied. It has been shown that $F_{(n)} = 0$ (namely, $A_n(z)$=0) when the nth DFLW is anti-symmetrical. Thus the field of $\boldsymbol{u}^{(2f)}$ is only symmetrical.[29–31] Under the condition $c_{(l)}^{(f)} = c_{(n)}^{(2f)}$, the value of the algebraic expression in { } in Eq. (12) is 1, and then the solution of the nth DFLW component that linearly grows with propagation distance can be given by

$$\boldsymbol{u}_{(n)}^{(2f)}(y,z) = \frac{F_{(n)}z}{4P_{nn}} \times \boldsymbol{u}_{(n)}^{(2f)}(y)\exp[\mathrm{j}k_{(n)}^{(2f)}z]. \quad (13)$$

4. SHG of some types of guided waves

4.1. SHG of shear horizontal guided waves

It is known that the particle displacement of shear horizontal (SH) guided wave propagation is in parallel to the surface of the waveguide.[37] In general, each guided wave mode can be taken as superposition of partial bulk acoustic waves satisfying the corresponding boundary conditions. A SH guided wave mode can be represented by two shear waves that are reflected at the upper and lower boundaries of the solid plate. Modal analysis of waveguide excitation can effectively be employed to investigate the SHG of SH guided wave modes under second-order perturbation.[38,39]

If the excitation source of the SH wave mode is located at $z = 0$, and the mth SH wave mode with angular frequency ω is produced in the plate of thickness $2d$ as shown in Fig. 3, the solution to the mth SH wave mode can formally be expressed as

$$\boldsymbol{u}_{(m)\mathrm{Ti}} = u_{(m)\mathrm{Ti}}\hat{\boldsymbol{x}}\exp[\mathrm{j}(\boldsymbol{K}_{(m)\mathrm{Ti}} \cdot \boldsymbol{r} - \omega t)], \quad i = 1,2, \quad (14)$$

where $\hat{\boldsymbol{x}}$ is the unit vector along the ox axis and the subscript m denotes the ordinal of SH mode. $k_{(m)} = \omega/c_{(m)}$ in Fig. 3 is the oz axis component of $\boldsymbol{K}_{(m)\mathrm{T1}}$ and $\boldsymbol{K}_{(m)\mathrm{T2}}$. $c_{(m)}$ is the phase velocity of the mth SH mode.

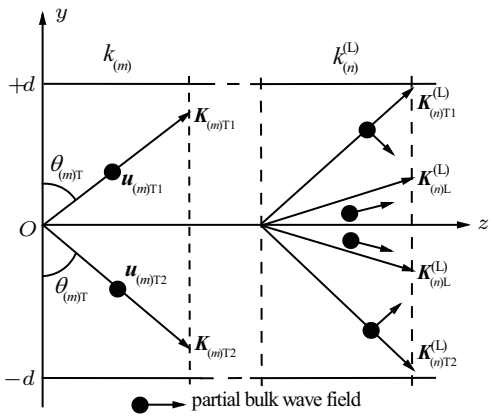


Fig. 3. Acoustic field of the mth SH wave mode and nth DFLW mode.[38]

The SHG of an SH wave mode can be analyzed by using the modal analysis approach. It is shown that the total second-harmonic field of a SH wave mode can be decomposed into a series of DFLW modes, due to the self- and cross-interactions of primary partial bulks waves. The field of a DFLW will have a cumulative growth effect versus propagation distance if its phase velocity exactly or approximately equals that of the primary SH wave mode.

Recently, Liu *et al.* used the mathematical approach to predict the cumulative behavior of the third-harmonic generation of SH guided waves with a hyperelastic material model.[40] In their investigation, reciprocity and normal mode expansion approach were used to find the ordinary differential equation for the modal participation factors. Results indicate that primary SH wave modes are holo-internal-resonant with the third-harmonic fields. Lissenden *et al.* developed an experimental procedure by using magnetostrictive transducers for measurement of the third harmonic of SH0 wave mode. The proposed setup was used to evaluate the localized microstructural evolution in an aluminum plate.[41]

Li *et al.* studied the nonlinear behavior of SH guided wave propagation using partial wave technique and normal mode expansion approach.[42] In their study, all of the phase matched SH modes in an isotropic plate were provided, as indicated in Fig. 4.[42]

Deng *et al.* studied the SHG of SH wave modes in a layered planar structure with imperfect interface.[43] The influences of interfacial properties on the effect of SHG by the SH guided wave were discussed in their study. The coordinates system associated to the structure with two solid layers is shown in Fig. 5, where d_i $(i = 1,2)$ denotes the solid layer thickness, and $\rho_{(i)}$ is the mass density. According to the partial wave analyses approach of guided wave modes, SH wave propagation in the structures shown in the layered structure

can be decomposed into four partial plane shear waves that have the same wave vector components along the oz axis.

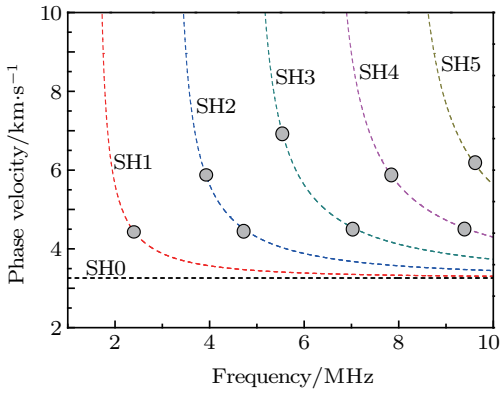


Fig. 4. (color online) SH guided wave dispersion curves and phase matched SH wave modes with 1 mm thickness.[42]

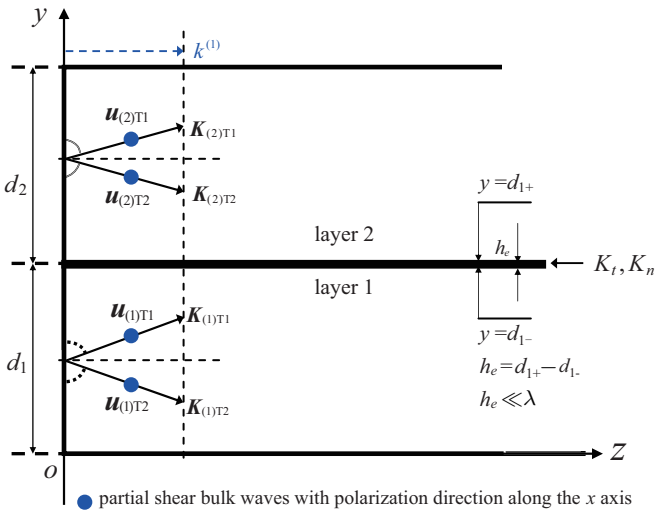


Fig. 5. (color online) Layered planar structure with the SH guided wave mode propagation.[43]

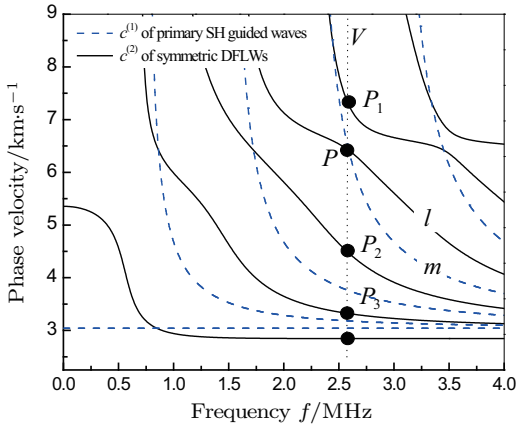


Fig. 6. (color online) Phase velocity dispersion curves for primary SH wave modes and the symmetric DFLWs in an aluminum sheet.[43]

The analyses indicate that the second-harmonic field generated by primary SH wave propagation consists of a series of DFLW modes with both longitudinal and transverse wave components for the reason that the cross-interaction of two shear waves can generate double frequency longitudinal wave components. As shown in Fig. 6, at the condition of phase velocity matching between the primary SH mode and the DFLW component, the amplitude of the corresponding second harmonic has a cumulative effect with propagation distance. Meanwhile, the mismatching of phase velocity can remarkably decrease the SHG efficiency of primary SH guided wave propagation.

4.2. SHG of Lamb waves in an isotropic plate

Investigation of SHG of Lamb wave propagation in an isotropic plate was firstly studied by perturbation method and partial wave technique.[27] In addition, a straightforward analyses of SHG of Lamb wave propagation by perturbation method and normal modal analysis technique were separately reported by Deng[31] and de Lima *et al.*[32] Srivastava *et al.* reported the possibility of the existence of anti-symmetric or symmetric second-harmonic Lamb wave modes.[44] Recently, this subject was also studied by using displacement gradient-based formation during the procedure of modal expanding analysis.[45,46]

To analyze the second-order solution of Lamb wave propagation, the normal model analysis approach is used. The total second harmonic field can be written as

$$\boldsymbol{u}_2 = \frac{1}{2}\sum_m A_m(z)\boldsymbol{u}_m(y)\exp(-\mathrm{j}2\omega t). \tag{15}$$

The solution of $A_m(z)$ in Eq. (15) with the source condition $\boldsymbol{u}_2 = 0$ at $z = 0$ is given by

$$A_m(z) = \bar{A}_m(z)\exp(2\mathrm{j}kz) - \bar{A}_m(0)\exp(-\mathrm{j}k_m^* z), \tag{16}$$

where

$$\bar{A}_m(z) = \frac{\mathrm{j}(f_m^{\mathrm{surf}} + f_m^{\mathrm{vol}})}{4P_{mn}(k_m^* - 2k)}, \quad k_n^* \neq 2k, \tag{17}$$

$$\bar{A}_m(z) = \frac{(f_m^{\mathrm{surf}} + f_m^{\mathrm{vol}})}{4P_{mm}}z, \quad k_m^* = 2k. \tag{18}$$

Here $\boldsymbol{u}_2$ is the displacement field function, z is the wave propagation distance, and $A_m(z)$ is the corresponding expansion coefficient, which is the second-order modal amplitude to be determined. The terms f_m^{surf} and f_m^{vol} are respectively defined as the complex external power due to the surface traction and the volume force generated by propagation of primary Lamb waves.

Based on the above analyses, it is found that second-harmonic amplitude grows linearly with propagation direction, when $k_m^* = 2k$ (synchronism) and $f_m^{\mathrm{surf}} + f_m^{\mathrm{vol}} \neq 0$ (nonzero power flux). If the selected wave mode satisfies the two conditions, the second-harmonic amplitude will have a cumulative effect versus propagation distance. In practice, interest is focused on the case where the second harmonic generated grows with propagation distance, since the cumulative second

harmonic plays a dominant role in the second-harmonics field after primary wave propagates a certain distance.[47]

The symmetric (S) modes, anti-symmetric (A) modes, and symmetric DFLW (D) modes are shown in Fig. 7, where the phase velocity matching modes can be found in the crossing points. The symmetric properties of DFLW modes will be discussed in Section 6. The frequencies along with corresponding phase velocities of different types of Lamb wave modes that can be used to generate cumulative second-harmonic waves have been discussed by Matsuda and Biwa.[48] It is important to note that the second-harmonic field of Lamb wave propagation can be considered as superposition of a series of DFLW components. However, most researchers focus on the DFLW component that has the same phase velocity as primary Lamb wave mode since only the DFLW mode with a proper phase velocity matching can remain in the second-harmonic field after propagating some distance, while all the other DFLW modes can be ignored due to destructive interference with each other.

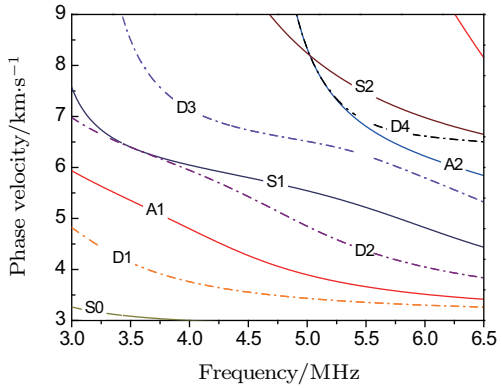


Fig. 7. (color online) Dispersion curves of primary Lamb waves and the symmetric DFLWs for a given aluminum plate with 1 mm thickness.[47]

4.3. SHG of Lamb waves in a layered planar structure

SHG of Lamb wave propagation in a two-layered solid waveguide was studied by combining the modal analyses approach and the nonlinear reflection of acoustic waves at interfaces.[49–51] A straightforward and convenient analytical expression of cumulative second harmonic of Lamb wave propagation in this layered structure was provided. To illustrate the theoretical model, nonlinear Lamb wave propagation in a two-layered waveguide made of two different materials denoted by M_i with thickness of d_i ($i = 1, 2$) was shown in Fig. 8. The oy axis is normal to the interface and the oz axis is along the interface of M_1 and M_2. The partial bulk acoustic waves constituting the primary Lamb wave with frequency f and ordinal l were denoted by the displacement fields $\boldsymbol{U}_{(i)\mathrm{L}q}^{(f,l)}$ and $\boldsymbol{U}_{(i)\mathrm{T}q}^{(f,l)}$ ($i = 1, 2$; $q = 1, 2$), where the subscript $(i) = (1)$ or (2) of $\boldsymbol{U}$ corresponds to the layer M_1 and M_2, T or L in $\boldsymbol{U}$ means that the corresponding quantity is associated with the transverse or longitudinal wave, respectively.

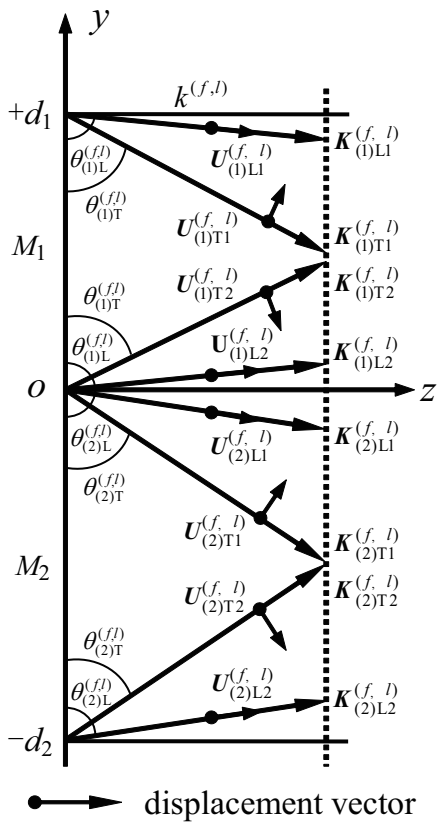


Fig. 8. The wave vectors and displacement fields of partial plane bulk acoustic waves constituting the lth primary Lamb wave.[51]

A modal analysis method was used to analyze the waveguide excitation. The second-harmonic field of Lamb wave propagation in the structure shown in Fig. 8 can be expressed as

$$\boldsymbol{U}^{(2f,n)} = \sum_n A_n(z)\boldsymbol{U}_{(i)}^{(2f,n)}(y), \tag{19}$$

with

$$\boldsymbol{U}_{(i)}^{(2f,n)}(y) = \begin{cases} \exp[\mathrm{j}k^{(2f,n)}z]\sum\limits_{q=1}^{2}[\boldsymbol{U}_{(1)\mathrm{L}q}^{(2f,n)} + \boldsymbol{U}_{(1)\mathrm{T}q}^{(2f,n)}], & 0 < y < d_1, \\ \exp[\mathrm{j}k^{(2f,n)}z]\sum\limits_{q=1}^{2}[\boldsymbol{U}_{(2)\mathrm{L}q}^{(2f,n)} + \boldsymbol{U}_{(2)\mathrm{T}q}^{(2f,n)}], & -d_2 < y < 0, \end{cases} \tag{20}$$

where $\boldsymbol{U}_{(i)}^{(2f,n)}(y)$ is the displacement field function of the nth DFLW mode. The modal expansion coefficient $A_n(z)$ can be determined as

$$\left[\frac{\partial}{\partial z} - \mathrm{j}k^{(2f,n)}\right] A_n(z) = \frac{1}{4P_{nn}}[f_n^{\mathrm{surf}}(z) + f_n^{\mathrm{vol}}(z)], \tag{21}$$

with

$$\begin{aligned} f_n^{\mathrm{surf}}(z) &= 2\mathrm{j}\omega\tilde{\boldsymbol{U}}_{(1)}^{(2f,n)}(y)\cdot\boldsymbol{P}_{s(1)}^{(2f)}\cdot\hat{\mathrm{y}}\big|_0^{d_1} \\ &\quad + 2\mathrm{j}\omega\tilde{\boldsymbol{U}}_{(2)}^{(2f,n)}(y)\cdot\mathrm{P}_{s(2)}^{(2f)}\cdot\hat{\mathrm{y}}\big|_{-d_2}^{0}, \end{aligned} \tag{22}$$

$$\begin{aligned} f_n^{\mathrm{vol}}(z) &= 2\mathrm{j}\omega\int_0^{d_1}\tilde{\boldsymbol{U}}_{(1)}^{(2f,n)}(y)\cdot\boldsymbol{F}_{b(1)}^{(2f)}\,\mathrm{d}y \\ &\quad + 2\mathrm{j}\omega\int_{-d_2}^{0}\tilde{\boldsymbol{U}}_{(2)}^{(2f,n)}\times(y)\cdot\boldsymbol{F}_{b(2)}^{(2f)}\,\mathrm{d}y, \end{aligned} \tag{23}$$

and

$$P_{nn} = \mathrm{Re}\left\{\int_0^{d_1}\left[-\frac{1}{2}\frac{\tilde{\partial}}{\partial t}\boldsymbol{U}_{(1)}^{(2f,n)}(y)\cdot\boldsymbol{T}_{(1)}^{(2f,n)}(y)\cdot\boldsymbol{z}\right]\mathrm{d}y + \int_{-d_2}^{0}\left[-\frac{1}{2}\frac{\tilde{\partial}}{\partial t}\boldsymbol{U}_{(2)}^{(2f,n)}(y)\cdot\boldsymbol{T}_{(2)}^{(2f,n)}(y)\cdot\boldsymbol{z}\right]\mathrm{d}y\right\}, \quad (24)$$

where $f_n^{\mathrm{surf}}(z)$ or $f_n^{\mathrm{vol}}(z)$ is the forcing function due to the coupling between $\boldsymbol{F}_{b(i)}^{(2f)}$ and $\boldsymbol{U}_{(i)}^{(2f,n)}(y)$, or due to the coupling between $\boldsymbol{P}_{b(i)}^{(2f)}$ and $\boldsymbol{U}_{(i)}^{(2f,n)}(y)$, respectively. P_{nn} is the average power flow per unit width along the ox axis for the nth DFLW mode, and $\hat{\boldsymbol{z}}$ denotes the unit vector along the oz axis. $\boldsymbol{T}_{(i)}^{(2f,n)}(y)$ is the stress tensor associated with $\boldsymbol{U}_{(i)}^{(2f,n)}(y)$. Considering the initial condition of SHG, the formal solution of $A_n(z)$ can be obtained as

$$A_n(z) = \frac{[f_n^{\mathrm{surf}}(z)+f_n^{\mathrm{vol}}(z)]\exp[-2\mathrm{j}k^{(f,l)}z]}{4P_{mn}} \times\frac{\sin\{[k^{(f,l)}-k^{(2f,n)}/2]\}}{[k^{(f,l)}-k^{(2f,n)}/2]} \times\exp[\mathrm{j}(k^{(f,l)}-k^{(2f,n)}/2)z]\times\exp[\mathrm{j}k^{(2f,n)}z]. \quad (25)$$

It shows that $A_n(z)$ is linearly proportional to propagation distance z under the condition of $k^{(f,l)} = k^{(2f,n)}/2$, which represents the phase velocity matching between the lth primary Lamb wave and the nth DFLW component.

Cumulative SHG of Lamb wave propagation in a solid plate contacting a liquid layer was also analyzed by Deng.[52] In this investigation, a second-order perturbation and approach of nonlinear reflection of acoustic wave at an interface were employed to describe the physical process of SHG of Lamb wave propagation.

4.4. SHG of guided waves in anisotropic media

Compared with Lamb wave propagation in the isotropic plate, the strain energy function for a nonlinear elastic transversely isotropic material is expressed in terms of the five invariants of the Green–Lagrange strain tensor. The formal solution of second-harmonic field of guided wave propagation in anisotropic media was analyzed by Deng *et al.*[53,54] and the analytical results show that the efficiency of SHG of guided wave propagation can be significantly affected by the elastic anisotropy.

As shown in Fig. 9, the Lagrangian coordinates (a_1, a_2, and a_3) are established for an anisotropic solid plate and guided waves are assumed to propagate along the a_3 axis. The formal solution of displacement field of a guided wave mode with the angular frequency ω can be expressed as[54]

$$U_i = U_i(a_2)\exp[\mathrm{j}(ka_3-\omega t)], \quad i=1,2,3, \quad (26)$$

where the subscript $i = 1$, 2, or 3 corresponds to the component of displacement field along the a_1, a_2, or a_3 axis. As illustrated in Fig. 9, the elastic constants of the anisotropic material are originally defined in the a_1', a_2', a_3' coordinate system. The corresponding elastic constants of the material in the $a_1a_2a_3$ coordinate can be obtained via the rotation transformation determined by the rotation angles γ_1, γ_2, and γ_3.

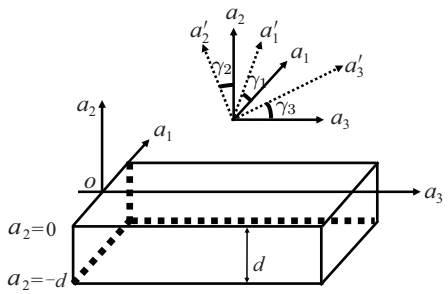


Fig. 9. Schematic representation of an anisotropic/piezoelectric solid plate.[54,57]

For anisotropic material, the component of the nonlinear term in Eq. (2) is given by

$$f_i = [C_{ijklmn}+\delta_{km}C_{ijln}+\delta_{im}C_{jnkl}+\delta_{ik}C_{jlmn}]\frac{\partial^2U_k\partial U_m}{\partial a_j\partial a_l\partial a_n}, \quad i,j,k,l,m,n=1,2,3, \quad (27)$$

where C_{ijkl} and C_{ijklmn} are the second- and third-order elastic constants in the $a_1a_2a_3$ coordinate, respectively. The second-order traction stress tensors at the top and bottom surfaces of the anisotropic plate can be written as

$$P_{ij} = \frac{1}{2}[C_{ijklmn}+\delta_{km}C_{ijln}+\delta_{im}C_{jnkl}+\delta_{ik}C_{jlmn}]\frac{\partial^2U_k\partial U_m}{\partial a_l\partial a_n}. \quad (28)$$

It is important to note that there is a factor $\exp[\mathrm{j}(2ka_3-2\omega t)]$ in f_i and P_{ij}.

Similar to the analysis of SHG of primary Lamb waves in an isotropic plate, the perturbation approximation and normal modal expansion approach are used in this problem. The second-harmonic field $\boldsymbol{u}_2$ of guided wave propagation in anisotropic plate can be expressed as

$$\boldsymbol{u}_2 = \frac{1}{2}\sum_m A_m(a_3)\times\boldsymbol{U}^{(2\omega,m)}(a_2)\times\exp(-\mathrm{j}2\omega t), \quad (29)$$

where $A_m(a_3)$ is the expansion coefficient of the mth double-frequency guided wave mode $\boldsymbol{U}^{(2\omega,m)}(a_2)$, which is determined by

$$\left[\frac{\partial}{\partial a_3}-\mathrm{j}k^{(2\omega,m)}\right]A_m(a_3) = \frac{f_m^{\mathrm{surf}}+f_m^{\mathrm{vol}}}{4P_{mm}}, \quad (30)$$

$$f_m^{\mathrm{vol}} = 2\mathrm{j}\omega\int_{-d}^{0}\sum_{i=1}^{3}[\tilde{U}_i^{(2\omega,m)}(a_2)\times f_i]\,\mathrm{d}a_2, \quad (31)$$

$$f_m^{\mathrm{surf}} = 2\mathrm{j}\omega\sum_{i=1}^{3}\left[\tilde{U}_i^{(2\omega,m)}(a_2)\cdot P_{i2}\right]\Big|_{a_2=-d}^{a_2=0}, \quad (32)$$

where $k^{(2\omega,m)}$ is the wave number of the mth double-frequency guided wave along the a_3 axis and P_{mm} is the average power flow of the mth double-frequency guided wave per unit width

along the a_1 axis. The initial condition for the SHG requires that $A_m(a_3)$ equal zero at $a_3 = 0$. Thus we have

$$A_m(a_3) = \frac{(f_m^{\text{surf}} + f_m^{\text{vol}})}{4P_{mm}} \frac{\sin[Dka_3]}{Dkd} \exp[\mathrm{j}k^{(2\omega,m)}a_3 + \mathrm{j}Dka_3], \quad (33)$$

where $D = 1 - k^{(2\omega,m)}/2k$. It shows that the amplitude of the second harmonic of primary guided wave propagation will grow with propagation distance a_3 under the condition of $D = 0$ or $D \approx 0$. The result of analysis given in Eqs. (29)–(33) is similar to the case where primary Lamb waves propagate in isotropic media.

Recently, Zhao *et al.* reported a theoretical study on the SHG of Lamb waves in composite.[55] The analysis shows that the efficiency of SHG can be determined by the propagation direction of Lamb waves in the composites. Li *et al.* provided an example of Lamb wave modes selection for generation of cumulative second harmonic in co-directional composites structure.[56]

4.5. SHG of guided waves in a piezoelectric plate

In piezoelectric material, piezoelectric and dielectric nonlinearities can be other sources for acoustic nonlinearity of primary guided wave propagation. Recently, Deng *et al.* studied the nonlinear behavior of ultrasonic guided wave propagation in a piezoelectric plate with nonlinear elastic, piezoelectric, and dielectric properties.[57] Generally, besides dispersion and multi-mode characteristics of guided wave propagation, the inherent coupling between the electric and mechanical fields in piezoelectric materials makes the theoretical analysis of SHG of guided waves much more complex than that in an isotropic elastic plate.

The Lagrangian coordinate system established for a single piezoelectric plate is shown in Fig. 9, where γ_1, γ_2, and γ_3 are the angles of orientation between the two coordinate systems $a_1a_2a_3$ and $a_1'a_2'a_3'$, and the elastic, piezoelectric, and dielectric constants of the piezoelectric material are originally defined under the coordinate system $a_1'a_2'a_3'$. The excitation sources for the generation of a series of double-frequency guided wave modes include bulk driving force components are indicated as $f_i^{(2f)}$ with double frequency. The second- and third-order elastic constants, second-order piezoelectric one, as well as the electrostrictive constant are involved into the expression of the bulk driving force $f_i^{(2f)}$.[58,59] Compared with non-piezoelectric material, there is a bulk charge density with the double frequency in piezoelectric material, denoted by $\rho^{(2f)}$. All the material constants in $f_i^{(2f)}$ and $\rho^{(2f)}$ should be transformed from the coordinate system $a_1'a_2'a_3'$ to $a_1a_2a_3$ as illustrated in Fig. 9. Besides the bulk driving force and bulk charge density in the interior of the piezoelectric plate, there are second-order stress tensors with the double frequency at the bottom and top surfaces of the piezoelectric plate, denoted as

$$P_{ij}^{(2f)} = \frac{1}{2}M_{ijklmn}\frac{\partial U_k}{\partial a_l}\frac{\partial U_m}{\partial a_n} - \frac{1}{2}d_{klij}\frac{\partial \varphi}{\partial a_k}\frac{\partial \varphi}{\partial a_l} + (f_{kijlm} + \delta_{il}e_{kmj})\frac{\partial U_l}{\partial a_m}\frac{\partial \varphi}{\partial a_k}, \quad (34)$$

and second-order surface charge density, written as

$$\sigma^{(2f)} = \frac{1}{2}\varepsilon_{2jk}\frac{\partial \varphi}{\partial a_j}\frac{\partial \varphi}{\partial a_k} + \frac{1}{2}(f_{2jklm} + \delta_{jl}e_{2km}) \times \frac{\partial U_j}{\partial a_k}\frac{\partial U_l}{\partial a_m} - d_{2jkl}\frac{\partial \varphi}{\partial a_j}\frac{\partial U_k}{\partial a_l}, \quad (35)$$

where φ is the electrical potential of the fundamental frequency, and M_{ijklmn} is defined by $c_{ijklmn} + \delta_{km}c_{ijln} + \delta_{im}c_{jnkl} + \delta_{ik}c_{jlmn}$ (i, j, k, l, m, $n = 1, 2, 3$). The constant e_{kmj} is a second-order piezoelectric one. It should be noted that the electrostrictive constant d_{klij} is related both to elasto-optic and electrostrictive effects, and that the third-order piezoelectric constant f_{kijlm} is related to the electroacoustic effect.

The second-order terms, $f_i^{(2f)}$, $\rho^{(2f)}$, $P_{ij}^{(2f)}$, and $\sigma^{(2f)}$, can provide a complete and accurate description for the SHG effect.[57] According to the modal analysis approach for waveguide excitation, these second-order terms can be regarded as excitation sources for generation of a series of double frequency guided wave modes. Thus, the field of the SHG by primary guided wave propagation (U_i, φ) can formally be expressed by the summation of these double frequency guided waves, i.e.,

$$U_i^{(2)} = \sum_m A_m(a_3) \cdot U_i^{(2f,m)}(a_2),$$
$$\varphi^{(2)} = \sum A_m(a_3) \cdot \varphi^{(2f,m)}(a_2), \quad (36)$$

where $U_i^{(2f,m)}(a_2)$ ($i = 1,2,3$) and $\varphi^{(2f,m)}(a_2)$ are respectively the a_i-axis displacement component and the electrical potential of the guided wave mode (with the driving frequency $2f$ and the order m), and $A_m(a_3)$ is the corresponding expansion coefficient. Based on the reciprocity relation and the orthogonality of guided waves, the equation governing $A_m(a_3)$ is given by

$$\left[\frac{\partial}{\partial a_3} - \mathrm{j}k^{(2f,m)}\right] A_m(a_3) = \frac{f_m^{\text{surf}} + f_m^{\text{vol}}}{4P_{mm}}, \quad (37)$$

with[57]

$$f_m^{\text{vol}} = 2\mathrm{j}\omega \int_{-d}^{0} [\tilde{U}_i^{(2f,m)}(a_2) \cdot f_i^{(2f)}]\,\mathrm{d}a_2 - \mathrm{j}2\omega \int_{-d}^{0} [\tilde{\varphi}^{(2f,m)}(a_2) \cdot \rho^{(2f)}]\,\mathrm{d}a_2, \quad (38)$$

$$f_m^{\text{surf}} = 2\mathrm{j}\omega\, [\tilde{U}_i^{(2f,m)}(a_2) \cdot P_{i2}^{(2f)}]\Big|_{a_2=-d}^{a_2=0} + 2\mathrm{j}\omega[\tilde{\varphi}^{(2f,m)}(a_2) \cdot \sigma^{(2f)}]\Big|_{a_2=-d}^{a_2=0}, \quad (39)$$

where P_{mm} is the average power flow per unit width along with the a_1 axis for the mth double frequency guided wave and

$k^{(2f,m)}$ is the a_3-axis component of the wave vectors. Considering an initial condition for SHG of primary guided wave propagation, i.e., $A_m(a_3) = 0$ when $a_3 = 0$, $A_m(a_3)$ can formally be given by

$$A_m(a_3) = \frac{A_m}{4}\frac{\sin[Dka_3]}{Dkd}\exp[\mathrm{j}k^{(2f,m)}a_3 + \mathrm{j}Dka_3], \quad (40)$$

where $A_m = (f_m^{\mathrm{surf}} + f_m^{\mathrm{vol}})d\exp(-2\mathrm{j}ka_3)/P_{mm}$. When $A_m \neq 0$ and $D = 0$, $A_m(a_3)$ can be written as $A_m(a_3) = (A_m/4d)a_3\exp[\mathrm{j}k^{(2f,m)}a_3]$, which means that the second-harmonic amplitude will increase with propagation distance a_3. When $A_m \neq 0$ and $D \neq 0$, there will be a beat effect for the amplitude of the mth guided wave with propagation distance and its contribution to $U_i^{(2)}$ and $\varphi^{(2)}$ can be negligible.

For a given set of orientation angles (γ_1, γ_2, γ_3), the primary guided wave propagating in the piezoelectric plate with the specific electrical boundary conditions at $a_2 = -d$ and 0 (see Fig. 9) can be selectively generated to ensure $A_m \neq 0$ and $D = 0$. In this way, the mth double frequency guided wave component will grow with propagation distance, and the obvious second-harmonic signals of primary guided wave propagation can be observed. When changes in the electrical boundary condition take place, the analysis given in Ref. [57] indicates that the efficiency of SHG by primary guided wave propagation will be remarkably influenced. This provides a means to regulate the SHG efficiency by changing the electrical boundary conditions.

4.6. SHG of primary guided waves in tube-like structures

de Lima *et al.* theoretically studied the elastic wave in waveguides with arbitrary cross-section media.[60] They reported the harmonics generation of ultrasonic guided wave propagation in cylindrical rods and shells, based on the perturbation method and normal mode decomposition technique which was suggested by Auld.[3] Practically, unlike the case of guided wave propagation in plate-like structures where the diffusion of energy for primary wave propagation makes it difficult for long range detection, the guided wave propagation in tube-like structures provides a more efficient approach to detect material nonlinearity due to its less energy diffusion.

The normal modal expansion analysis shown in Section 3 is applied to a cross-sectional area of any shape. For the tube-like structure as shown in Fig. 10, the particle displacement components of primary wave mode propagating along the z axis would be[60]

$$u_1^r = u_r(r)\cos(n\theta)\exp[\mathrm{j}(kz - \omega t)], \quad (41)$$
$$u_1^\theta = u_\theta(r)\sin(n\theta)\exp[\mathrm{j}(kz - \omega t)], \quad (42)$$
$$u_1^z = u_z(r)\cos(n\theta)\exp[\mathrm{j}(kz - \omega t)], \quad (43)$$

where the circumferential order is for $n = 0, 1, 2, \ldots$. For axisymmetric modes, $n = 0$, and $n \geq 1$ for the flexural modes. The flexural modes with $n = 1$ are called first-order flexural modes. Generally, the terms (u_1^r, u_1^θ, and u_1^z) depended on the type of waveguide and family of modes.

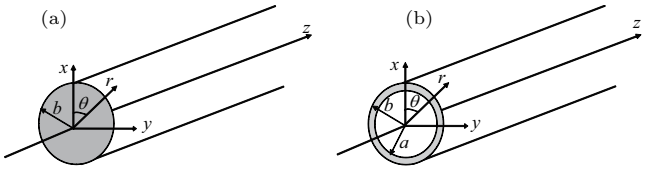


Fig. 10. Schematic of cylindrical waveguides (a) rod and (b) pipe.[60]

Accompanying propagation of primary wave mode (u_1^r, u_1^θ, u_1^z), there are second-order bulk driving force $\boldsymbol{f}^{(2)}(r,\theta)$ within the waveguide and second-order driving traction $\boldsymbol{s}^{(2)}(r,\theta)\big|_{r=a,b}$ at the surfaces $r = a$, b. Within a second-order perturbation, the second-harmonic field $\boldsymbol{u}_2$ of primary wave mode (u_1^r, u_1^θ, u_1^z) can be decomposed into a series of double frequency guided waves generated by $\boldsymbol{f}^{(2)}(r,\theta)$ and $\boldsymbol{s}^{(2)}(r,\theta)\big|_{r=a,b}$, i.e., $\boldsymbol{u}_2 = \sum_m A_m(z)\boldsymbol{u}_m(r,\theta)$, where $\boldsymbol{u}_m(r,\theta)$ is the displacement field function of the mth double frequency guided wave and the corresponding traction stress is denoted by $\boldsymbol{s}_m(r,\theta)$, and $A_m(z)$ is the modal expansion coefficient. The formal expression of $A_m(z)$ is given by

$$A_m(z) = \frac{(f_m^{\mathrm{surf}} + f_m^{\mathrm{vol}})}{4P_{mm}}\frac{\sin[Dkz]}{Dk}\exp[\mathrm{j}k^{(2\omega,m)}z + \mathrm{j}Dkz], \quad (44)$$

where $D = 1 - k^{(2\omega,m)}/2k$ and $k^{(2\omega,m)}$ is the wave number of the mth double frequency guided wave. For cylindrical rod (see Fig. 10), the expressions of P_{mm}, f_n^{surf}, and f_n^{vol} are shown as

$$P_{mm} = -\frac{\mathrm{j}\omega}{8}\int_0^{2\pi}\int_0^b \{[\tilde{\boldsymbol{u}}_m(r,\theta)\cdot\boldsymbol{s}_m(r,\theta) - \boldsymbol{u}_m(r,\theta)\cdot\tilde{\boldsymbol{s}}_m(r,\theta)]\cdot\boldsymbol{z}\}r\mathrm{d}r\mathrm{d}\theta, \quad (45)$$
$$f_m^{\mathrm{surf}} = -\mathrm{j}\omega b\int_0^{2\pi}\left[\tilde{\boldsymbol{u}}_m(b,\theta)\cdot\boldsymbol{s}^{(2)}(b,\theta)\cdot\hat{\boldsymbol{r}}\right]\mathrm{d}\theta, \quad (46)$$
$$f_m^{\mathrm{vol}} = \mathrm{j}\omega\int_0^b\int_0^{2\pi}\left[\tilde{\boldsymbol{u}}_m(r,\theta)\cdot\boldsymbol{f}^{(2)}(r,\theta)\right]r\mathrm{d}r\mathrm{d}\theta. \quad (47)$$

For the cylindrical shell, they can be expressed as

$$P_{mm} = -\frac{\mathrm{j}\omega}{8}\int_0^{2\pi}\int_a^b \{[\tilde{\boldsymbol{u}}_m(r,\theta)\cdot\boldsymbol{s}_m(r,\theta) - \boldsymbol{u}_m(r,\theta)\cdot\tilde{\boldsymbol{s}}_m(r,\theta)]\cdot\hat{\boldsymbol{z}}\}r\mathrm{d}r\mathrm{d}\theta, \quad (48)$$
$$f_m^{\mathrm{surf}} = \mathrm{j}\omega b\int_0^{2\pi}\left[\tilde{\boldsymbol{u}}_m(b,\theta)\cdot\boldsymbol{s}^{(2)}(b,\theta)\cdot\hat{\boldsymbol{r}}\right]\mathrm{d}\theta - \mathrm{j}\omega a\int_0^{2\pi}\left[\tilde{\boldsymbol{u}}_m(a,\theta)\cdot\boldsymbol{s}^{(2)}(a,\theta)\cdot\boldsymbol{r}\right]\mathrm{d}\theta, \quad (49)$$
$$f_m^{\mathrm{vol}} = \mathrm{j}\omega\int_a^b\int_0^{2\pi}\left[\tilde{\boldsymbol{u}}_m(r,\theta)\cdot\boldsymbol{f}^{(2)}(r,\theta)\right]r\mathrm{d}r\mathrm{d}\theta. \quad (50)$$

Here $\hat{\boldsymbol{r}}$ and $\hat{\boldsymbol{z}}$ are the unit vectors along the radial and axial directions, respectively. If we submit Eqs. (41)–(43) under the condition of $n = 0$ into Eqs. (45)–(47) or Eqs. (48)–(50), the condition $f_m^{\mathrm{surf}} + f_m^{\mathrm{vol}} \neq 0$ (nonzero power flux) will always be

satisfied. It shows that all axisymmetric modes, including longitudinal modes and torsional modes in a tube-like structure, can be used to generate cumulative second harmonics under the condition of synchronism, when the secondary waves have the same phase velocity as that of primary wave mode (i.e., $D = 0$ in Eq. (44)). Similarly, for the SHG of flexural mode propagation, under the condition of $n \neq 0$, the theoretical analyses can be used to choose the suitable double frequency flexural mode with non-zero power flux from primary wave mode to second harmonic ones.

Theoretical studies of the conditions for the existence of longitudinal or flexural waves in nonlinear, isotropic rods were presented by Srrivastava *et al.*,[61–63] who applied the analytical solutions in rail tracks for the potential measurement of thermal stress in welded rail. Liu *et al.* studied the interaction of axisymmetric torsional and longitudinal guided waves in circular cylinders.[64] Li, *et al.* investigated the axisymmetric guided waves modes in pipe and applied the phase matched longitudinal guided wave modes to evaluate the thermal damage.[65,66] Recently, numerical studies of nonlinear guided waves in uniform waveguides with arbitrary cross section were conducted by Zuo *et al.* and the SHG of guided waves in a steel rectangular bar was studied using the proposed numerical model.[67]

4.7. SHG of circumferential guided waves

Circumferential guided wave (CGW) is another kind of fundamental wave mode that propagates along the circumference of the circular tubes. Recently, Gao and Deng *et al.* established a theoretical model to analyze the SHG of CGW propagation in a circular tube with isotropic, homogeneous, and dispersionless features.[68–70] The cylindrical coordinates for analyzing CGW propagation were shown in Fig. 11.

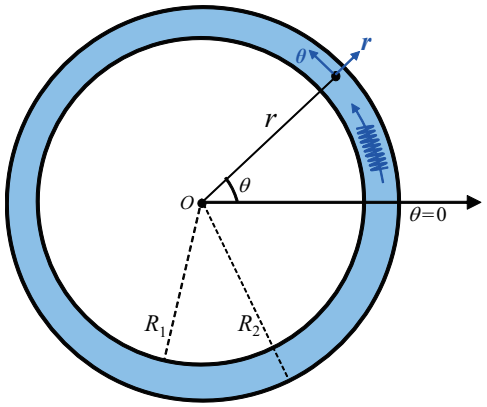


Fig. 11. (color online) Lagrangian cylindrical coordinates (r, θ) for analyzing CGW propagation.[70]

The displacement field of the primary CGW mode propagating along the circumference of the circular tube can be expressed as

$$\boldsymbol{u}_1 = \boldsymbol{u}_1(r)\exp[\mathrm{j}n^{(1)}\theta - \mathrm{j}\omega t], \tag{51}$$

where $n^{(1)}$ is the dimensionless angular wave number of the CGW mode. The components of bulk driving force in the interior of the circular tube and surface stress are the sources for the generation of a series of double frequency CGW modes under second order perturbation approximation, denoted as $f_q^{(2)}$ and $P_{qr}^{(2)}$ $(q = r, \theta)$, which can be expressed in the cylindrical coordinates as[70]

$$f_r^{(2)} = \frac{1}{r}\frac{\partial(rP_{rr}^{(2)})}{\partial r} + \frac{1}{r}\frac{\partial(P_{r\theta}^{(2)})}{\partial \theta} - \frac{\partial(P_{\theta\theta}^{(2)})}{\partial r}, \tag{52}$$

$$f_\theta^{(2)} = \frac{1}{r}\frac{\partial(rP_{\theta r}^{(2)})}{\partial r} + \frac{1}{r}\frac{\partial(P_{\theta\theta}^{(2)})}{\partial \theta} + \frac{\partial(P_{r\theta}^{(2)})}{\partial r}, \tag{53}$$

and

$$\begin{aligned} P_{rr}^{(2)} &= a\left[(\frac{1}{r}\frac{\partial U_r}{\partial \theta} - \frac{U_\theta}{r})^2 + (\frac{\partial U_\theta}{\partial r})^2\right] \\ &\quad + 2d\left(\frac{1}{r}\frac{\partial U_\theta}{\partial \theta} + \frac{U_r}{r}\right)\frac{\partial U_r}{\partial r} \\ &\quad + b\left(\frac{\partial U_r}{\partial r}\right)^2 + d\left(\frac{1}{r}\frac{\partial U_\theta}{\partial \theta} + \frac{U_r}{r}\right)^2 \\ &\quad + e\left(\frac{1}{r}\frac{\partial U_r}{\partial \theta} - \frac{U_\theta}{r}\right)\frac{\partial U_\theta}{\partial r}, \end{aligned} \tag{54}$$

$$\begin{aligned} P_{\theta\theta}^{(2)} &= a\left[\left(\frac{1}{r}\frac{\partial U_r}{\partial \theta} - \frac{U_\theta}{r}\right)^2 + \left(\frac{\partial U_\theta}{\partial r}\right)^2\right] \\ &\quad + b\left(\frac{1}{r}\frac{\partial U_\theta}{\partial \theta} + \frac{U_r}{r}\right)^2 \\ &\quad + 2d\frac{\partial U_r}{\partial r}\left(\frac{1}{r}\frac{\partial U_\theta}{\partial \theta} + \frac{U_r}{r}\right) + d\left(\frac{\partial U_r}{\partial r}\right)^2 \\ &\quad + e\left(\frac{1}{r}\frac{\partial U_r}{\partial \theta} - \frac{U_\theta}{r}\right)\frac{\partial U_\theta}{\partial r}, \end{aligned} \tag{55}$$

$$\begin{aligned} P_{r\theta}^{(2)} &= 2a\left[\left(\frac{1}{r}\frac{\partial U_r}{\partial \theta} - \frac{U_\theta}{r}\right)\left(\frac{\partial U_r}{\partial r} + \frac{1}{r}\frac{\partial U_\theta}{\partial \theta} + \frac{U_r}{r}\right)\right] \\ &\quad + e\left[\frac{\partial U_\theta}{\partial r}\left(\frac{\partial U_r}{\partial r} + \frac{1}{r}\frac{\partial U_\theta}{\partial \theta} + \frac{U_r}{r}\right)\right], \end{aligned} \tag{56}$$

$$\begin{aligned} P_{\theta r}^{(2)} &= 2a\left[\frac{\partial U_\theta}{\partial r}\left(\frac{\partial U_r}{\partial r} + \frac{1}{r}\frac{\partial U_\theta}{\partial \theta} + \frac{U_r}{r}\right)\right] \\ &\quad + e\left[\left(\frac{1}{r}\frac{\partial U_r}{\partial \theta} - \frac{U_\theta}{r}\right)\left(\frac{\partial U_r}{\partial r} + \frac{1}{r}\frac{\partial U_\theta}{\partial \theta} + \frac{U_r}{r}\right)\right], \end{aligned} \tag{57}$$

where $U_r = \boldsymbol{r}\cdot\boldsymbol{u}_1$, $U_\theta = \hat{\boldsymbol{\theta}}\cdot\boldsymbol{u}_1$, and $\hat{\boldsymbol{r}}$ and $\hat{\boldsymbol{\theta}}$ are the unit vectors along the radial and circumferential direction, respectively. The parameters a, b, d, and e in Eqs. (54)–(57) are defined in Ref. [70]. The second-harmonic field of primary CGW propagation generated by $f_q^{(2)}$ and $P_{qr}^{(2)}$ $(q = r, \theta)$ can be written as

$$\boldsymbol{u}_2 = \sum_m A_m(\theta) \times \boldsymbol{u}^{(2f,m)}(r), \tag{58}$$

where $A_m(\theta)$ is the expansion coefficient of the mth double frequency CGW, determined by

$$\left[\frac{\partial}{\partial \theta} - \mathrm{j}n^{(2)}\right]A_m(\theta) = \frac{1}{4P_{mm}}\left[f_m^{\mathrm{surf}} + f_m^{\mathrm{vol}}\right], \tag{59}$$

where $n^{(2)}$ and P_{mm} are the dimensionless angular wave number of the mth double frequency CGW and the corresponding average power flow per unit width perpendicular to the tube section. Due to the bulk driving force $f_q^{(2)}$ $(q = r, \theta)$ and surface stress $P_{qr}^{(2)}$ $(q = r, \theta)$, f_m^{surf} and f_m^{vol} can be expressed as

$$f_m^{\text{vol}} = \int_{R_1}^{R_2} \left\{ \frac{\partial \tilde{\boldsymbol{u}}^{(2f,m)}(r)}{\partial t} \cdot \left[\hat{\boldsymbol{r}} f_r^{(2)} + \hat{\boldsymbol{\theta}} f_\theta^{(2)} \right] \right\} \mathrm{d}r, \quad (60)$$

$$f_m^{\text{surf}} = \left\{ \left(\frac{\tilde{\boldsymbol{u}}^{(2f,m)}(r)}{\partial t} \cdot \hat{\boldsymbol{r}} \right) P_{rr}^{(2)} + \left(\frac{\partial \tilde{\boldsymbol{u}}^{(2f,m)}(r)}{\partial t} \cdot \hat{\boldsymbol{\theta}} \right) P_{\theta r}^{(2)} \right\} \Bigg|_{r=R_1}^{r=R_2}. \quad (61)$$

The solution to $A_m(\theta)$ in Eq. (59) is given by

$$A_m(\theta) = \left[\frac{\sin(\Delta n \theta)}{\Delta n} \exp(\mathrm{j} \Delta n \theta) \right] \times \frac{\left[f_m^{\text{surf}} + f_m^{\text{vol}} \right]}{4 P_{mm}} \exp[\mathrm{j} n^{(2)} \theta], \quad (62)$$

where $\Delta n = [n^{(1)} - n^{(2)}/2$ is used to describe the dispersion degree between the primary mode and the mth double frequency CGW. It can be found that the amplitude of the mth double frequency CGW will grow linearly along the tube circumference under the condition of $\Delta n = 0$ and $f_m^{\text{surf}} + f_m^{\text{vol}} \neq 0$, and can be written as

$$A_m(\theta) = \frac{\left(f_m^{\text{surf}} + f_m^{\text{vol}} \right)}{4 P_{mm}} \theta \exp[\mathrm{j} n^{(2)} \theta]. \quad (63)$$

Obviously, the theoretical results obtained for SHG of primary CGWs are similar to those of ultrasonic guided wave propagation in plate-like structures.

5. Features of nonlinear guided wave propagation

Proper mode tuning with physically based feature is highly demanded to enhance the efficiency of the generation and reception of second harmonics. The phase matched guided wave modes could be found in the dispersion curves. The key concept of nonlinear guided wave test is to use those modes with a good phase matching associated with significant energy transmission from the fundamental frequency wave mode to the second harmonic. Selecting certain modes among all the phase matched ones can play a significant role to improve the sensitivity of the detection of material nonlinearity in practice. Li *et al.* studied the nonlinear feature of phase matched Lamb wave modes for comparison of efficiency of SHG.[71]

The displacement of guided wave propagation in an isotropic plate with traction free boundary condition can be decomposed into in-plane and out-of-plane contributions, and each contribution can be divided into symmetric and anti-symmetric parts.[72] The ratio of the displacement amplitudes of primary wave (U_f) and second harmonic (U_{2f}) can be represented as

$$\frac{U_f^2}{U_{2f}} = \frac{8}{\beta k_l^2 z} \frac{\cosh^2(pd)}{\cosh(2pd)} \left(1 - \frac{k^2 + q^2}{2k^2} \right), \quad (64)$$

where $p = \sqrt{k^2 - k_l^2}$, $q = \sqrt{k^2 - k_t^2}$, and k, k_l, and k_t are the wave numbers of Lamb wave, bulk longitudinal wave, and bulk transverse wave, respectively. z is the wave propagation distance and d is the plate thickness.

Therefore, the nonlinear parameter for symmetric Lamb wave modes can be represented by in-plane displacement on the surface as

$$\beta_{\text{L,s}} = \frac{A_2}{A_1^2} \frac{8}{k_l^2 z} \frac{\cosh^2(pd)}{\cosh(2pd)} \left(1 - \frac{k^2 + q^2}{2k^2} \right), \quad (65)$$

where A_2 and A_1 are the in-plane displacement amplitude for the second harmonic and primary wave of symmetric Lamb wave modes on the plate surface. The nonlinear parameter for anti-symmetric modes can also be derived with the same procedure as

$$\beta_{\text{L,a}} = \frac{A_2}{A_1^2} \frac{8}{k_l^2 z} \frac{\sinh^2(pd)}{\cosh(2pd)} \left(1 - \frac{k^2 + q^2}{2k^2} \right). \quad (66)$$

Using the same method, the nonlinear parameters of Lamb wave propagation can be represented by the out-of-plane displacement on the surface as

$$\beta_{\text{L,s}} = \frac{A_2}{A_1^2} \frac{i8}{k_l^2 z} \frac{p}{k} \frac{\sinh^2(pd)}{\sinh(2pd)} \left(1 - \frac{2k^2}{k^2 + q^2} \right), \quad (67)$$

$$\beta_{\text{L,a}} = \frac{A_2}{A_1^2} \frac{i8}{k_l^2 z} \frac{p}{k} \frac{\cosh^2(ph)}{\sinh(2ph)} (1 - \frac{2k^2}{k^2 + q^2}), \quad (68)$$

where $\beta_{\text{L,s}}$ and $\beta_{\text{L,a}}$ are the nonlinear parameters for symmetric and anti-symmetric Lamb wave modes, respectively. It is important to note that the cumulative second- harmonic field is symmetric even the primary wave mode is anti-symmetric mode.

The formulas in Eqs. (65)–(68) show that the acoustic nonlinear parameters for Lamb waves are associated with the driving frequency, material properties, and geometric information of the waveguide. The nonlinear feature of a Lamb wave mode can be affected by the mode type, driving frequency of the incident signal, the material properties, and the geometric information of the waveguide. The formula derived can help us to predict the efficiency of SHG. However, the efficiency of SHG is only one factor for nonlinear guided wave test. In experimental tests, the overall considerations of various factors for second-harmonic measurement should be a concern and they will be discussed in the next section.

The characteristics of various phase matched Lamb wave modes were also discussed by Müller *et al.*[73] and Matlack *et al.*,[73] who investigated the SHG of different phase matched Lamb wave modes in nonlinear elastic plates. The actual rate

of SHG is important for the measurement of the second harmonic with high signal-to-noise ratio. In their work, the ratio of second-harmonic amplitude to the square of the primary-wave amplitude is used to quantify the rate of SHG. Although the well-phase-matched guided wave modes can generate a cumulative second-harmonic wave, there is a need to study the physical insight of the nonlinear feature among different phase matched guided wave modes for the higher efficiency of higher harmonic generation. Studies of nonlinear features of various phase matched guided wave modes are necessary for comparison of SHG efficiency.

6. Discussions on two disputed issues

6.1. Symmetry of second-harmonic fields of Lamb waves

The symmetry of second-harmonic fields of Lamb wave propagation was investigated by Deng,[29–31] de Lima *et al.*,[32] and Chillara *et al.*[75] Based on the results of these existing investigations, it can be concluded that a symmetric primary guided wave mode can generate a symmetric secondary wave mode. However, their controversial conclusion is about the symmetry of the secondary wave mode in the case of the primary antisymmetric guided wave mode. De Lima *et al.* state that a primary mode can generate a secondary mode only with the same symmetry, which means that an antisymmetric primary mode can generate an antisymmetric but not a symmetric secondary mode.[32] In contrast, the analytical expressions and numerical analyses of the second-harmonic field were provided by Deng, and the results obtained indicate that the cumulative second harmonic is symmetrical regardless of whether primary Lamb wave propagation is symmetrical or antisymmetrical.[29–31] Müller *et al.* also investigated the symmetry properties of the second harmonic of Lamb wave propagation,[73] and the symmetry properties for the second-harmonic field of primary Lamb waves were obtained when the primary Lamb wave mode was either symmetric or antisymmetric. The analytical solution of second harmonics of primary Lamb waves shows that only the symmetric second-harmonic modes at double frequency exist, even if the antisymmetric Lamb wave modes are selected as the primary guided waves. It can be concluded that neither symmetric nor antisymmetric primary Lamb wave mode can generate an antisymmetric Lamb wave mode at double frequency.

6.2. Influence of group velocity mismatching

In order to ensure generation of cumulative second harmonic of guided waves, it is well accepted that the conditions of phase velocity matching and non-zero power flux from primary mode to secondary mode should be satisfied.[29–32] In addition, some researchers pointed out that the requirement of group velocity matching between the primary guided wave mode and secondary ones is also needed for generation of a cumulative second harmonic.[76–78] However, this idea is still in dispute.[79,80]

The theoretical analysis of SHG of guided waves propagation at the condition of non-matched group velocity of primary mode and secondary ones was firstly reported by Deng *et al.*[79,80] Figure 12 shows the mode pair that satisfies the phase matching condition, while the group velocity of primary wave mode ($c_{\mathrm{g}}^{[f]}$) is higher than that of secondary one ($c_{\mathrm{g}}^{[2f]}$). The process of generation of the second harmonic under the condition of phase velocity matching ($c_{\mathrm{p}}^{[f]} = c_{\mathrm{p}}^{[2f]}$) and group velocity mismatching ($c_{\mathrm{g}}^{[f]} > c_{\mathrm{g}}^{[2f]}$) is schematically illustrated in Fig. 13, where $c_{\mathrm{p}}^{[f]}$ and $c_{\mathrm{p}}^{[2f]}$ are the phase velocity of the primary Lamb wave and DFLW, respectively. The tone-burst signal of DFLW will be generated when the tone burst of the primary Lamb wave is excited at the position Tx, assuming that the time-of-flight of the DFLW tone burst from z_{p} to Rx is $(z-z_{\mathrm{p}})/c_{\mathrm{g}}^{[2f]}$, while the time-of-flight for the primary wave tone burst from z_0 to z_{p} is $z_{\mathrm{p}}/c_{\mathrm{g}}^{[f]}$. Figure 13 indicates that at the position Rx, the time range of the envelope of the DFLW tone burst is from $z/c_{\mathrm{g}}^{[f]}$ to $z/c_{\mathrm{g}}^{[2f]}+\tau$, where the corresponding envelope function is denoted by $A_{2f}(t)$. The cumulative second- harmonic field mainly dependent on the DFLW mode due to $c_{\mathrm{p}}^{[f]} = c_{\mathrm{p}}^{[2f]}$ can be generated. Based on the analysis shown in Fig. 13, the physical process of SHG can be clearly illustrated in the time range $z/c_{\mathrm{g}}^{[f]} \sim z/c_{\mathrm{g}}^{[2f]}+\tau$. From the time range of $z/c_{\mathrm{g}}^{[f]}$ to $z/c_{\mathrm{g}}^{[f]}+\tau$, the overlapping degree of the DFLW tone burst will increase linearly with time. Thus, the second-harmonic amplitude increases linearly with time in this time range. From the time range of $z/c_{\mathrm{g}}^{[f]}+\tau$ to $z/c_{\mathrm{g}}^{[2f]}$, the overlapping degree of the DFLW tone burst generated is kept unchanged, and thus the amplitude is kept constant in this specified time range. From the time range of $z/c_{\mathrm{g}}^{[2f]}$ to $z/c_{\mathrm{g}}^{[2f]}+\tau$, the overlapping degree of the DFLW tone burst decreases linearly with time. Actually, the second harmonic generated in the time range from $z/c_{\mathrm{g}}^{[f]}+\tau$ to $z/c_{\mathrm{g}}^{[2f]}$ is equivalent

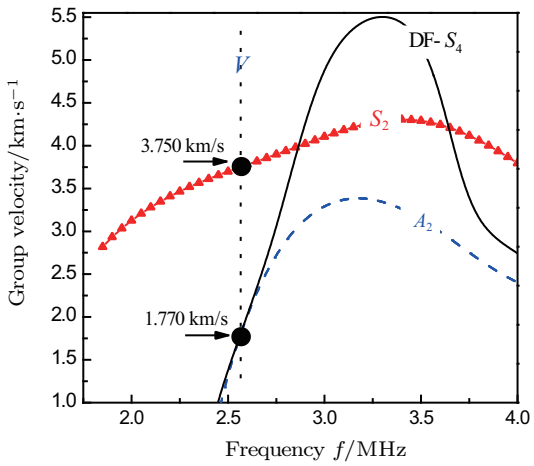


Fig. 12. (color online) Group velocity dispersion curves for primary Lamb waves and DFLWs.[79]

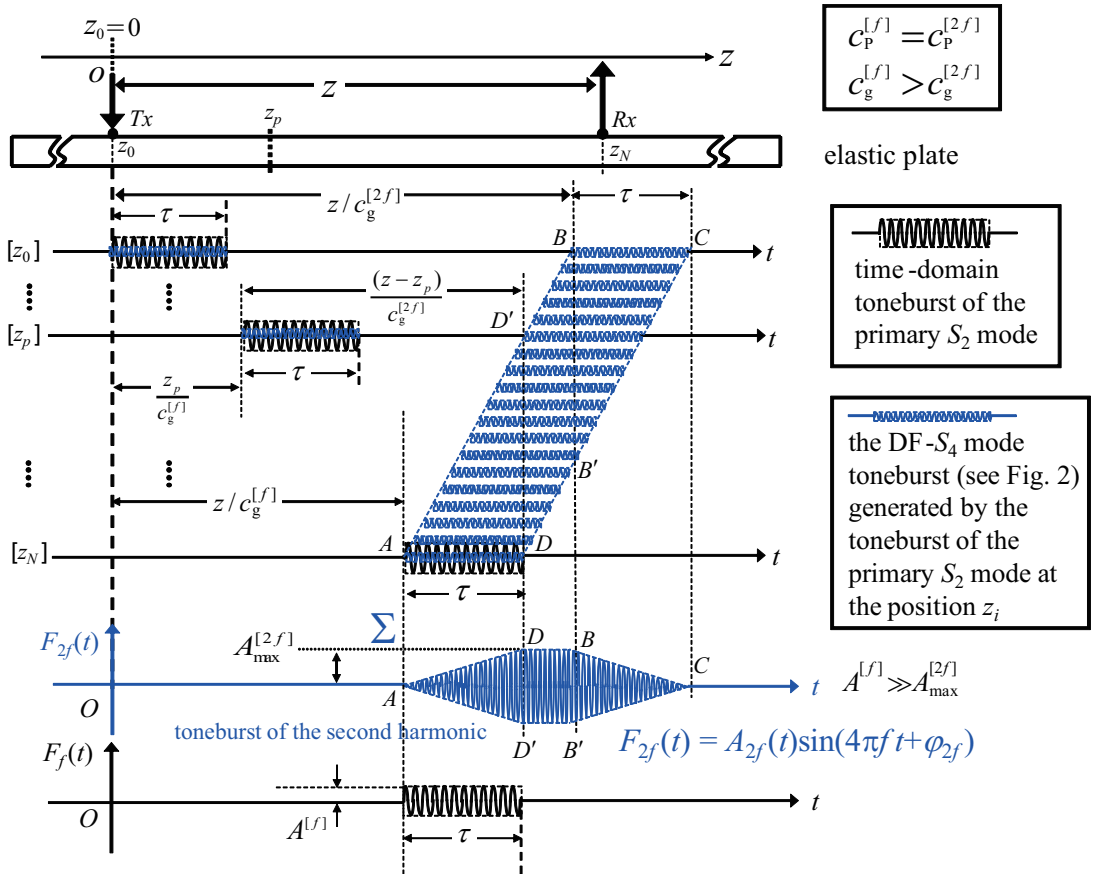


Fig. 13. (color online) Process of generation of the second harmonic under the condition of $c_p^{[f]}=c_p^{[2f]}$ and $c_g^{[f]}>c_g^{[2f]}$.[79]

to the second harmonic generated by a continuous Lamb wave passing through the path z. The result of the analysis shown in Fig. 13 has been confirmed by the experiment.[79]

Recently, Xiang *et al.* further studied the generation of cumulative second harmonic by guided wave propagation with group velocity mismatching by numerical and experimental methods.[81] As illustrated in their results, it is found that the cumulative effect of SHG with propagation distance can be obtained for the phase matched mode pair under the condition of group velocity mismatching. Thus, it can be concluded that the integrated amplitude of the second-harmonic signal (i.e., $\int_{z/c_g^{[f]}}^{\tau+z/c_g^{[2f]}} A_{2f}(t)\,\mathrm{d}t$ in Fig. 13), which can be used to quantify the SHG efficiency, grows linearly with propagation distance even when the group velocity matching condition is not satisfied.

7. Conclusion and prospect

We present a review of the theoretical studies on SHG of guided wave propagation in solid media. The perturbation approach is widely used to solve the nonlinear wave equation with boundary condition, and to obtain the solutions of the primary wave mode as well as the secondary one arising from the body forces and surface tractions generated by nonlinearities at twice the fundamental frequency. Within a second-order perturbation approximation, nonlinear reflection of acoustic waves at interfaces and normal modal expansion are two means to derive the solutions of the secondary wave modes at twice the fundamental frequency. The theoretical analysis of acoustic fields of primary and secondary wave modes can be used to find the conditions for SHG with a cumulative effect versus propagation distance. Cumulative SHG of ultrasonic guided wave propagation in different structures/materials is theoretically discussed. The theoretical study of SHG of guided wave modes provides more insight into choosing the proper mode pair for better excitability/receivability in detecting material's nonlinearity. Two typically disputed issues for nonlinear guided wave propagation are clarified. This paper is of significance for comprehensively understanding the current status of theoretical investigations of SHG by ultrasonic guided wave propagation.

Due to the complicated physical mechanism of SHG of ultrasonic guided wave propagation, there are still some research challenges that need to be addressed. (i) The physical insight into the nonlinear features among different guided wave modes is still obscure. It is worth further investigation to select certain wave modes among all the phase-velocity-matched ones, which can increase the efficiency of SHG of primary guided waves, and can improve the sensitivity of the detection of material nonlinearity. (ii) Generally, the physi-

cal process of SHG of ultrasonic guided waves is described based on the classical nonlinear constitutive relation. However, the intrinsic mechanism of the nonlinear response of ultrasonic guided waves due to the complex dependence of local or volumetric nonlinearity is not yet well understood. (iii) The current testing strategy based on the SHG of ultrasonic guided wave propagation is generally applicable to test over a region rather than a specific location. How to develop an approach based on the nonlinear ultrasonic guided waves for locating the local nonlinearity (e.g. degradation/damage) is a difficult issue to be addressed.

From the authors' viewpoint, future tendencies of research in nonlinear guided waves may include the following. (i) Due to the complexity and difficulty of the experimental examinations of nonlinear ultrasonic guided waves, the strategy of numerical simulations will undoubtedly play an increasing role in checking the relevant theoretical predictions. (ii) The physical process of SHG of ultrasonic guided waves in isotropic plates or plate-like structures has been widely analyzed. In the next step, further investigations will be focused on the nonlinear guided waves propagating in either anisotropic, inhomogeneous media or complex waveguide structures. (iii) Due to the similar advantages of nonlinear frequency mixing of bulk acoustic waves (e.g. great flexibility in selecting wave modes, frequencies, and propagation directions), analyses of nonlinear frequency mixing response of ultrasonic guided waves will undoubtedly attract more and more attention.

References

[1] Achenbach J D 1973 *Wave Propagation in Elastic Solids* (Amsterdam: North-Holland Press)
[2] Rose J L 1999 *Ultrasonic Waves in Solid Media* (New York: Cambridge University Press)
[3] Auld B A 1990 *Acoustic Fields and Waves in Solids* (Malabar: Kreiger Press)
[4] Shui Y and Solodov I 1988 *J. Appl. Phys.* **64** 6155
[5] Ginsberg J H 1979 *J. Acoust. Soc. Am.* **65** 1127
[6] Zhou S and Shui Y 1992 *J. Appl. Phys.* **72** 5070
[7] Korneeva V and Demčenko A 2014 *J. Acoust. Soc. Am.* **135** 591
[8] Nagy P B 1998 *Ultrasonics* **36** 375
[9] Cantrell J H and Yost W T 2001 *Int. J. Fatigue* **23** 487
[10] Jhang K Y 2000 *IEEE Trans. Ultrason. Ferroelectr. Freq. Control* **47** 540
[11] Kim J Y, Jacobs L J, Qu J and Littles J W 2006 *J. Appl. Phys.* **99** 124913
[12] Li W, Cho Y, Lee J and Achenbach J D 2013 *Exp. Mech.* **53** 775
[13] Li W, Cho Y and Hyun S 2012 *Int. J. Precis. Eng. Man.* **13** 935
[14] Xiang Y X, Zhu W J, Deng M X and Xuan F Z 2016 *Chin. Phys. B* **25** 024303
[15] Xiang Y X, Deng M X, Liu C J and Xuan F Z 2015 *J. Appl. Phys.* **117** 214903
[16] Xiang Y X, Deng M X and Xuan F Z 2014 *J. Nondestruct. Eval.* **33** 279
[17] Buck O 1976 *IEEE Trans. Ultrason. Ferroelectr. Freq. Control* **23** 346
[18] Deng M 2000 *J. Sound Vib.* **230** 507
[19] Deng M 2005 *Acta Acustica* **30** 0371 (in Chinese)
[20] Rose J L 2004 *Key Eng. Mater.* **270** 14
[21] Love M, Alleyne D N and Cawley P 1998 *Ultrasonics* **36** 147
[22] Rose J L 2002 *J. Press. Vessel Tech.* **124** 273
[23] Cho Y 2000 *IEEE Trans. Ultrason. Ferroelectr. Freq. Control* **47** 591
[24] Murnaghan F D 1951 *Finite Deformation of an Elastic Solid* (Wiley)
[25] Landau L D and Lifschitz E M 1956 *Theory of Elasticity* (Oxford: Pregamon Press)
[26] He X, Shui Y, Mao Y W and Jiang W 1996 *Appl. Phys. Lett.* **69** 614
[27] Deng M 1996 *Acta Acustica* **21** 429 (in Chinese)
[28] Deng M 1997 *Acta Acustica* **22** 182 (in Chinese)
[29] Deng M 1999 *J. Appl. Phys.* **85** 3051
[30] Deng M 1996 *Jpn. J. Appl. Phys.* **35** 4004
[31] Deng M 2003 *J. Appl. Phys.* **94** 4152
[32] de Lima W J N and Hamilton M F 2003 *J. Sound Vib.* **265** 819
[33] Mao Y, Shui Y, Jiang W, Lu Z and Wu W 1989 *Appl. Phys. Lett.* **55** 2394
[34] Zhou S and Shui Y 1992 *J. Appl. Phys.* **72** 5070
[35] Deng M 1997 *J. Appl. Phys.* **82** 1026
[36] Deng M 2008 *Chin. J. Acoust.* **27** 1
[37] Li W and Cho Y 2015 *Sensor. Actuat. A-Phys.* **232** 251
[38] Deng M 1998 *J. Appl. Phys.* **84** 3500
[39] Deng M and Liu Z 2002 *Appl. Phys. Lett.* **81** 1916
[40] Liu Y, Chillara V K, Lissenden C J and Rose J L 2013 *J. Appl. Phys.* **114** 114908
[41] Lissenden C J, Liu Y, Choi G W and Yao X 2013 *J. Nondestruct. Eval.* **33** 178
[42] Li W, Choi J and Cho Y 2015 *Phys. Proce.* **70** 451
[43] Deng M and Xiang Y X 2013 *J. Appl. Phys.* **106** 024902
[44] Srivastava A and di Scalea F L 2009 *J. Sound Vib.* **323** 932
[45] ChillaraV K and Lissenden C J 2012 *J. Appl. Phys.* **111** 124909
[46] Liu Y, ChillaraV K and Lissenden C J 2013 *J. Sound Vib.* **332** 4517
[47] Cho Y 2012 *J. Nondestruct. Eval.* **31** 324
[48] Matsuda N and Biwa S 2011 *J. Appl. Phys.* **109** 094903
[49] Deng M 2005 *NDT&E Inter.* **38** 85
[50] Deng M 2006 *Appl. Phys. Lett.* **88** 221902
[51] Xiang Y X, Deng M and Xuan F Z 2009 *J. Appl. Phys.* **106** 024902
[52] Deng M 2000 *Acustica Acta Acoustica* **86** 239
[53] Deng M 2007 *J. Sound Vib.* **308** 201
[54] Deng M 2008 *Appl. Phys. Lett.* **92** 111910
[55] Zhao J, ChillaraV K, Ren B, Cho H, Qiu J and Lissenden C J 2016 *J. Appl. Phys.* **119** 064902
[56] Li W, Cho Y and Achenbach J D 2012 *Smart Mater. Struct.* **21** 085019
[57] Deng M and Xiang Y X 2015 *Ultrasonics* **61** 121
[58] Mcmahon D H 1968 *J. Acoust. Soc. Am.* **44** 1007
[59] Ljamov V E 1972 *J. Acoust. Soc. Am.* **52** 199
[60] de Lima W J N and Hamilton M F 2005 *Wave Motion* **41** 1
[61] Srivastava A and di Scalea F L 2010 *J. Sound Vib.* **329** 1499
[62] Srivastava A, Salamone S and di Scalea F L 2010 *J. Acoust. Soc. Am.* **127** 2790
[63] Nucera C and di Scalea F L 2014 *J. Acoust. Soc. Am.* **136** 2561
[64] Liu Y, Khajeh E, Lissenden C J and Rose J L 2013 *J. Acoust. Soc. Am.* **133** 2541
[65] Li W and Cho Y 2014 *Exp. Mech.* **54** 1309
[66] Li W, Deng M and Cho Y 2016 *J. Comput. Acoust.* **24** 1650011
[67] Zuo P, Zhou Y and Fan Z 2016 *AIP Adv.* **6** 075207
[68] Gao G, Deng M and Li M 2015 *Acta Phys. Sin.* **64** 184303 (in Chinese)
[69] Deng M, Gao G and Li M 2015 *Chin. Phys. Lett.* **32** 124305
[70] Deng M, Gao G, Xiang Y X and Li M 2017 *Ultrasonics* **75** 209
[71] Li W, Cho Y and Achenbach J D 2010 *Rev. Prog. Quant. Nondestruct. Eval.* **1581** 662
[72] Viktorov I A 1967 *Rayleigh and Lamb Waves Physical Theory and Application* (New York: Plenum Press)
[73] Müller M F, Kim J Y, Qu J and Jacobs L J 2010 *J. Acoust. Soc. Am.* **127** 2141
[74] Matlack K H, Kim J Y, Jacobs L J and Qu J 2011 *J. Appl. Phys.* **109** 014905
[75] Chillara V and Lissenden C J 2013 *Ultrasonics* **53** 862
[76] Bermes C, Kim J Y, Qu J and Jacobs L J 2008 *Mech. Syst. Sig. Process.* **22** 638
[77] Pruell C, Kim J Y, Qu J and Jacobs L J 2009 *Smart Mater. Struct.* **18** 035003
[78] Pruell C, Kim J Y, Qu J and Jacobs L J 2008 *NDT&E Inter.* **42** 199
[79] Deng M, Xiang Y and Liu L 2011 *J. Appl. Phys.* **109** 113525
[80] Deng M and Xiang Y 2010 *Chin. Phys. B* **19** 114302
[81] Xiang Y, Zhu W, Deng M, Xuan F and Liu C 2016 *Europhys. Lett.* **116** 34001